doi:10.1093/brain/awv006 BRAIN 2015: 138; 1009–1022 | 1009

BRAIN
A JOURNAL OF NEUROLOGY

Rapidly progressive Alzheimer's disease features distinct structures of amyloid-β

Mark L. Cohen,[1,2] Chae Kim,[1] Tracy Haldiman,[1] Mohamed ElHag,[1] Prachi Mehndiratta,[3] Termsarasab Pichet,[3] Frances Lissemore,[3] Michelle Shea,[3] Yvonne Cohen,[1,2] Wei Chen,[1,2] Janis Blevins,[1,2] Brian S. Appleby,[3,4] Krystyna Surewicz,[5] Witold K. Surewicz,[5] Martha Sajatovic,[3,4] Curtis Tatsuoka,[3] Shulin Zhang,[1] Ping Mayo,[6] Mariusz Butkiewicz,[6] Jonathan L. Haines,[6] Alan J. Lerner[3] and Jiri G. Safar[1,2,3]

Genetic and environmental factors that increase the risk of late-onset Alzheimer disease are now well recognized but the cause of variable progression rates and phenotypes of sporadic Alzheimer's disease is largely unknown. We aimed to investigate the relationship between diverse structural assemblies of amyloid-β and rates of clinical decline in Alzheimer's disease. Using novel biophysical methods, we analysed levels, particle size, and conformational characteristics of amyloid-β in the posterior cingulate cortex, hippocampus and cerebellum of 48 cases of Alzheimer's disease with distinctly different disease durations, and correlated the data with *APOE* gene polymorphism. In both hippocampus and posterior cingulate cortex we identified an extensive array of distinct amyloid-β_{42} particles that differ in size, display of N-terminal and C-terminal domains, and conformational stability. In contrast, amyloid-β_{40} present at low levels did not form a major particle with discernible size, and both N-terminal and C- terminal domains were largely exposed. Rapidly progressive Alzheimer's disease that is associated with a low frequency of *APOE* e4 allele demonstrates considerably expanded conformational heterogeneity of amyloid-β_{42}, with higher levels of distinctly structured amyloid-β_{42} particles composed of 30–100 monomers, and fewer particles composed of < 30 monomers. The link between rapid clinical decline and levels of amyloid-β_{42} with distinct structural characteristics suggests that different conformers may play an important role in the pathogenesis of distinct Alzheimer's disease phenotypes. These findings indicate that Alzheimer's disease exhibits a wide spectrum of amyloid-β_{42} structural states and imply the existence of prion-like conformational strains.

1 Department of Pathology, Case Western Reserve University School of Medicine, 2085 Adelbert Rd, Cleveland, OH 44106, USA
2 National Prion Disease Pathology Surveillance Centre, Case Western Reserve University School of Medicine, 2085 Adelbert Rd, Cleveland, OH 44106, USA
3 Department of Neurology, Case Western Reserve University School of Medicine, 2085 Adelbert Rd, Cleveland, OH 44106, USA
4 Department of Psychiatry, Case Western Reserve University School of Medicine, 2085 Adelbert Rd, Cleveland, OH 44106, USA
5 Department of Physiology and Biophysics, Case Western Reserve University School of Medicine, 2085 Adelbert Rd, Cleveland, OH 44106, USA
6 Department of Epidemiology and Biostatistics, Case Western Reserve University School of Medicine, 2085 Adelbert Rd, Cleveland, OH 44106, USA

Correspondence to: Jiri G. Safar,
Department of Pathology,
Case Western Reserve University,
2085 Adelbert Rd,
Cleveland,
OH.
E-mail: jiri.safar@case.edu

Keywords: Alzheimer; β-amyloid; structure; progression rate

Received June 24, 2014. Revised November 24, 2014. Accepted November 26, 2014. Advance Access publication February 16, 2015

Abbreviations: CDI = conformation-dependent immunoassay; PPC = precuneus/posterior cingulate cortex (Brodmann area 23 and 31)

Introduction

The genetic and environmental factors linked to the increased risk of developing late-onset Alzheimer disease are well established (Selkoe, 2011; Schellenberg and Montine, 2012). We recently described a novel subgroup of patients with rapidly progressive dementia mimicking prion diseases which, after exhaustive neuropathological investigation and prion protein gene sequencing, was concluded to be rapidly progressive Alzheimer's disease (Chitravas *et al.*, 2011). Data from all of the cases with rapidly progressive Alzheimer's disease collected independently at prion centres in Germany, Japan, Spain and France have uniformly confirmed the presence of differentiating clinical characteristics and a low frequency of e4 alleles in the *APOE* gene, while the autosomal dominant history of dementia or comorbidity was absent (Schmidt *et al.*, 2010, 2011, 2012, 2013; Chitravas *et al.*, 2011). The pathogenetic mechanisms leading to these variable progression rates and phenotypes of Alzheimer's disease are unknown (Schellenberg and Montine, 2012).

Extensive analysis of ageing brain samples indicates that the pathological processes underlying Alzheimer's disease begin early in isolated anatomical structures of the brain, and then spread through neuronal projections (Braak and Del Tredici, 2013). In transgenic mice models of Alzheimer's disease and tauopathy, this process can be accelerated by intracerebral injection of preformed misfolded amyloid-β or tau. Moreover, studies show that different structural conformers of misfolded proteins have varying potency to accelerate the pathology (Kane *et al.*, 2000; Guo and Lee, 2013). The data suggest a prion-like intercellular propagation of misfolding; and as synthetic amyloid-β is significantly less active in this 'seeding' effect than amyloid-β of brain origin, the data also imply a conformational and biological plasticity, which is the fundamental basis for vastly differing phenotypes (strains) of prion diseases (Meyer-Luehmann *et al.*, 2006; Prusiner, 2012, 2013; Safar, 2012*a*, *b*). These findings have raised some questions, specifically, whether the structure of different conformers and assemblies of brain amyloid-β contribute to varying progression rates of the Alzheimer's disease, and whether subtle differences in the conformation of amyloid-β may be responsible for the distinct disease phenotypes (Kabir and Safar, 2014). Therefore, structural characterization and differentiation of amyloid-β spectrum in the wide range of phenotypes and progression rates of Alzheimer's disease should provide clues into the pathogenetic role of amyloid-β, and specifically different conformers (assemblies) in the amyloid cascade. Identification of differential and well-characterized mechanistic determinants of Alzheimer's disease variants could help inform future treatments that are customized and focused on relevant pathologic factors.

Using advanced conformation-sensitive techniques (Safar *et al.*, 1998; Kim *et al.*, 2011, 2012; Safar, 2012*a*, *b*), we investigated amyloid-β_{42} and amyloid-β_{40} peptides in the brains of Alzheimer's disease cases with variable disease progression tempo. Our findings described below demonstrate the remarkable structural diversity of brain amyloid-β_{42}—a characteristic that is not present in amyloid-β_{40}—and establish a link between particular conformers of amyloid-β_{42} and the fast progression rate of Alzheimer's disease.

Materials and methods

Ethics statement

All procedures were performed under protocols approved by the Institutional Review Board at Case Western Reserve University and University Hospitals Case Medical Centre in Cleveland, OH. In all cases, written informed consent for research was obtained from the patient or legal guardian, and the material used had appropriate ethical approval for use in this project. All patients' data and samples were coded and handled according to NIH guidelines to protect patients' identities.

Patients and clinical evaluations

The rapidly progressive Alzheimer's disease cohort was randomly selected from a group of 276 patients with a definitive diagnosis of rapidly progressive sporadic Alzheimer's disease who were referred to the National Prion Disease Pathology Surveillance Centre (NPDPSC) from 2002 to 2012 with a rapidly progressive dementia and a differential diagnosis of prion disease. In all cases, we were able to exclude familial or sporadic prion disease after sequencing the *PRNP* gene, conducting neuropathology and immunohistochemistry for the pathogenic prion protein (PrP^{Sc}), and molecular typing of PrP^{Sc} by western blots. Case records accumulated with standard NPDPSC protocol by trained personnel were analysed retrospectively. These records included medical charts, semi-structured telephone interviews of the prion surveillance centre personnel with patients and caregivers at the time of referral, EEG, MRI and laboratory results (Puoti *et al.*, 2012; Schmidt *et al.*, 2012). The criteria for inclusion into the rapidly progressive Alzheimer's disease cohort were: (i) initial referral to NPDPSC and classification as possible prion disease due to the clinical appearance in accordance with the consensus official criteria valid at the time of referral (Geschwind *et al.*, 2008; Puoti *et al.*, 2012; Schmidt *et al.*, 2012); (ii) decline in more than six Mini-Mental State Examination (MMSE) points per year and/or death within 3 years of initial neurological diagnosis of atypical dementia (Geschwind *et al.*, 2008; McKhann *et al.*, 2011; Schmidt *et al.*, 2012); (iii) absent autosomal dominant pattern of the dementia; (iv) absent pathogenic mutations

in the human prion protein (PrP) gene (*PRNP*); (v) neuropathology and immunohistochemistry of tau proteins and amyloid-β with unequivocal classification as sporadic Alzheimer's disease; (vi) absence of neuropathologic comorbidity; and (vii) distribution of means and proportions of demographic data within 95% confidence interval of the whole group, resulting in no difference in means and proportions between the randomly selected and all Alzheimer's disease cases in the NPDPSC database. Because there are no definite clinical criteria for rapidly progressive Alzheimer's disease (Schmidt *et al.*, 2010, 2011, 2012), and to prevent contamination of this cohort with outliers, for further studies we selected cases within the normal distribution interval of disease duration calculated as UQ + 1.5*IQR, where UQ is upper quartal, and IQR is inter-quartal range.

The cases with slowly progressive Alzheimer's disease were defined as those diagnosed between 2001 and 2013 at the Brain Health and Memory Centre of the Neurological Institute at University Hospitals Case Medical Centre, and brains were collected in the repository of the Department of Pathology at Case Western Reserve University (Tatsuoka *et al.*, 2013; Chien *et al.*, 2014). The criteria for inclusion in the slowly progressive Alzheimer's disease cohort were: (i) unequivocal clinical diagnosis of Alzheimer's disease (McKhann *et al.*, 2011); (ii) absent autosomal dominant pattern of dementia; (iii) unequivocal classification as Alzheimer's disease after detailed neuropathology and immunohistochemistry of tau proteins and amyloid-β; (iv) absence of concurrent clinical or neuropathologic comorbidity; and (v) the distribution of means and proportions of demographic data within 95% confidence interval of late-onset cases accumulated in National Alzheimer's Coordinating Centre (NACC) at the University of Washington between September 2005 and February 2013 (Beekly *et al.*, 2007). In all cases, the clinical diagnosis of probable slowly progressive and rapidly progressive Alzheimer's disease was confirmed by diagnostic histopathology (McKhann *et al.*, 2011). For comparison of disease durations, we used late onset autopsy-proven Alzheimer's disease cases submitted to the NACC database at the University of Washington (Beekly *et al.*, 2007). The control non-Alzheimer's disease group consisted of age- and sex-matched patients whose primary cause of death was lymphoma, carcinomatosis, or autoimmune disorder and the neuropathology ruled out prion disease, Alzheimer's disease, or other neurodegenerative disorder (Supplementary Table 2).

Sequencing of *PRNP*, *APOE*, *APP*, *PSEN1* and *PSEN2* genes

DNA was extracted from frozen brain tissues in all cases, and genotypic analysis of the *APOE* gene polymorphism and the *PRNP* coding region was performed as described (Parchi *et al.*, 1996, 2000; Safar *et al.*, 2005).

Illumina sequencing

The coding regions of *APP*, *PSEN1* and *PSEN2* were analysed using a TruSeq® Custom Amplicon kit generated using DesignStudio (www.Illumina.com). Parameters were selected for 425 base pair amplicons and the design was successful for *APP* and *PSEN1* but failed for exons 4 and 5 in *PSEN1*; for these exons we used Sanger sequencing. Paired end sequencing using a v3 600 cycle kit was performed on an Illumina MiSeq instrument (Illumina) with an output of 50 million paired end reads. All sequence reads for all genotypic samples were aligned to the human genome reference version 19. Genotypes of each base position were called with a minimum 20-times coverage. Minor and major allele frequencies were calculated for every variant of the sample population, and we identified intronic and exonic regions. Each variant was cross-referenced with the Alzheimer Disease and Frontotemporal Dementia Mutation Database (Cruts *et al.*, 2012) and the NHLBI Exome Sequencing Project (ESP) Exome Variant Server (EVS) (http://evs.gs.washington.edu/EVS/) for SNP occurrences in the genes *APP*, *PSEN1* and *PSEN2*.

Sanger sequencing

Screening for exons 4 and 5 in *PSEN1* were carried out by PCR followed by Sanger dideoxy sequencing (Sanger *et al.*, 1977). Exon-specific oligonucleotide primers flanking the two regions of interest were designed using Primer3 software (http://frodo.wi.mit.edu/) and obtained from IDT (www.idtdna.com). PCR amplification was performed with following exon specific primers: PSEN1_E04_F_aaccgttaccttgattctgctgag, PSEN1_E04_R_agccacactggctttgagaata, PSEN1_E05_F_gttggaggtggtaatgtggttgg, PSEN1_E05_R_acccaaccataagaagaacagggt. PCR products were purified from unincorporated primers and dNTPs using shrimp alkaline phosphatase and bi-directional DNA sequencing was performed using BigDye® Terminator v3.1 Cycle Sequencing Kit (Applied Biosystems) and pigtail primers. Unincorporated nucleotides and dye-labelled chain terminators were removed using Agencourt CleanSEQ kit (http://www.agencourt.com/documents/products/cleanseq/Agencourt_CleanSEQ_Protocol.pdf). Sequencing products were size fractionated by electrophoresis and detected in a 3730xl DNA Analyzer (Applied Biosystems). Sequencing analysis was performed using Mutation Surveyor Version 4.0.7 (Softgenetics). The data were compared to reference *PSEN1* sequence: NG_007386.2 GI:213511787.

Brain sampling

Coronal sections of human brain tissues were obtained at autopsy and stored at −80°C. Three 200–350 mg cuts of hippocampal, precuneus/posterior cingulate (PPC) cortex (Brodmann areas 23 and 31), and cerebellum were taken from each brain and used for molecular analyses. Slices of brain tissue weighing 200–350 mg were homogenized to a final 15% (w/v) concentration by three 75 s cycles with Mini-beadbeater 16 Cell Disrupter (Biospec) in Tris-buffered saline (TBS), pH 7.4, containing complete protease inhibitor cocktail (Roche Applied Science). Pre-adsorption was carried out with 0.6 ml of 10% homogenate containing 0.1% Sarkosyl and 1.5 mg magnetic beads coated with Protein A/G mixture or Streptavidin (Pierce) at 5°C for 1 h. The Sarkosyl was adjusted to a final 1% (v/v), the sample was re-homogenized by two cycles of 75 s, clarified at 500 *g* for 5 min, and aliquots of the supernatant were stored at −80°C for future analysis.

Western blots

SDS PAGE and western blots for amyloid-β were performed as described (Sherman and Lesne, 2011). Alternatively, the

transblots were denatured with a saturated vapour of 96% formic acid in an airtight chamber for 40 min (Safar *et al.*, 1993*b*). The PVDF filters were developed with 0.13 µg/ml of biotinylated mAb 6E10 (epitope human amyloid-β residues 1–16, Covance), or 0.2 µg/ml of peroxidase-labelled mAb 4G8 (epitope human amyloid-β residues 17–24, Covance). The densitometry of western blots was performed with ImageJ software.

Conformation-dependent immunoassay of amyloid-β_{40} and amyloid-β_{42}

The conformation-dependent immunoassay (CDI) for amyloid-β_{40} and amyloid-β_{42} is based on principles we developed for the measurement and characterization of prions (Supplementary Fig. 2A) (Safar *et al.*, 1998, 2002, 2005, 2008; Bellon *et al.*, 2003; McCutcheon *et al.*, 2005; Thackray *et al.*, 2007; Choi *et al.*, 2011*a*, *b*; Kim *et al.*, 2011, 2012). The measurement of both amyloid-β_{40} and amyloid-β_{42} in native and denatured states was performed with amplified luminescent proximity homogeneous assay (AlphaLISA®) technology platform (Perkin Elmer). Briefly, for detection of amyloid-β_{42} and amyloid-β_{40}, we used the donor and acceptor beads coated with mAb 82E1 specific for N-terminus (epitope human amyloid-β residues 10–17), and mAb specific for either C-terminus of amyloid-β_{42} (12F4), or C-terminus of amyloid-β_{40}, respectively (Perkin Elmer). The 96-well half-area white plates (Perkin Elmer) were first filled with 20 µl per well of 12.5 µg/ml of Acceptor beads and 1.25 nM biotinylated mAb. The thawed samples were sonicated with three 5 s cycles using Misonix Sonicator 4000 at 80% power output, and made into two 4 µl aliquots: native (N) and denatured (D). The native sample was mixed with 28 µl assay buffer (Perkin Elmer) and kept at room temperature; the second aliquot was denatured with 28 µl of final 7 M Gdn HCl at 80°C for 10 min. Both native and denatured aliquots were diluted with 80 µl of assay buffer, 5 µl loaded immediately onto the plate, and incubated at room temperature for 2 h. Next, 25 µl of 40 µg/ml of streptavidin-coated Donor beads were added per well and incubated for 1 h at room temperature. The fluorescence signals were measured by the multi-mode microplate reader PHERAstar Plus (BMG LabTech), by using the 'AlphaScreen' PHERAstar Plus software. Concentrations of the samples were calculated from the signal of denatured sample and standard dilution curve of amyloid-β_{40} and amyloid-β_{42} peptides, and are expressed in ng/ml of the original 10% brain homogenate. The ratio of denatured/native (D/N) signal is proportional to the concentration of N- and C-terminal epitopes that are hidden in native state due to the formation of the polymeric assemblies of misfolded proteins (Safar *et al.*, 1998; Kim *et al.*, 2011, 2012; Haldiman *et al.*, 2013).

Conformational stability assay of amyloid-β_{42}

The dissociation and denaturation of human amyloid-β_{42} was performed as described previously for prions (Supplementary Fig. 2B) (Safar *et al.*, 1998; Kim *et al.*, 2011, 2012; Haldiman *et al.*, 2013), with several modifications. The 15 µl aliquots of 10% brain homogenate in 15 tubes were treated with increasing concentrations of 8 M Gdn HCl in 0.25 M or 0.5 M increments. After 10 min incubation at 80°C, individual samples were rapidly diluted with Assay buffer (Perkin Elmer) containing diminishing concentrations of 8 M Gdn HCl, so that the final concentration in all samples was 2.0 M. The individual 5 µl aliquots were developed according to the AlphaLISA protocol with the final 0.2 M Gdn HCl in reaction mixture. The raw fluorescence signal was converted into the apparent fractional change of unfolding (Fapp) as follows: $F = (TRF_{OBS} - TRF_N) / (TRF_U - TRF_N)$ where TRF_{OBS} is the observed TRF value, and TRF_N and TRF_U are the TRF values for native and unfolded forms, respectively, at the given Gdn HCl concentration (Safar *et al.*, 1993*a*; Kim *et al.*, 2011, 2012; Haldiman *et al.*, 2013). To determine the difference in stability of amyloid-β_{42} between individual samples, the values of individual fractional change were subtracted ($\Delta F_{app} = F_{app}{}^1 - F_{app}{}^2$) and then fitted with a Gaussian model to estimate the proportion and average stability of differential conformers (Kim *et al.*, 2011, 2012).

Separation of amyloid-β particles by sedimentation velocity in sucrose gradient

Sucrose gradient sedimentation velocity separation was performed as described previously (Kim *et al.*, 2012; Haldiman *et al.*, 2013; Mays *et al.*, 2014). These conditions correspond to the adjusted proportionality constant k = 58.7 and angular velocity $\omega = 5236$ rad/s. Observed sedimentation coefficients S_{obs} were calculated from the formula $S_{obs} = k/(\omega^2 t)$, where t is the centrifugation time. The $S_{20,w}$ values for given angular velocity and sucrose density and viscosity were calculated as described (Prusiner *et al.*, 1978; Steensgaard *et al.*, 1992; Kim *et al.*, 2012). Alternatively, to estimate the sedimentation profiles in the gradient, we used the sedimented distance and particle density 1.35 g/ml (Wille and Prusiner, 1999) in standard plots of $s\omega^2 t$ for sucrose gradients provided by the rotor manufacturer (Beckman). The third approach to estimate the S values in the upper layers of sucrose gradient was calibration with bovine serum albumin (BSA, S = 4.4, MW = 67 kDa), alcohol dehydrogenase (ADH, S = 7.9, MW = 150 kDa), thyroglobulin monomer (TG, S = 12.0, MW = 335 kDa), and apoferritin (AF, S = 17.0, MW = 443 kDa) (Steensgaard *et al.*, 1992; Kim *et al.*, 2012). Finally, we established the S value for monomers, oligomers and fibrillar amyloid-β_{42} prepared according to standard protocols (Stine *et al.*, 2011) and verified the quaternary structure with atomic force microscopy.

Statistical analysis

Cumulative survival curves were constructed by the Kaplan–Meier method. Comparisons of survival curves among groups were carried out by the log rank (Mantel-Cox) test. In the comparison of different patient groups, *P*-values were calculated using ANOVA and two-tailed Fisher's exact test. A mixed model analysis was conducted to compare the rapidly progressive and slowly progressive Alzheimer's disease unfolding curves across all Gdn HCl levels. Subject level random intercepts were included, to reflect within subject correlation. All the statistical analyses were performed using SPSS 21 software (SPSS Inc., Chicago, IL).

Results

Demographics, sequencing of genes, and comparative pathology in rapidly and slowly progressive Alzheimer's disease cohorts

We reviewed records of 276 patients with rapidly progressive or atypical dementia referred to the National Prion Disease Pathology Surveillance Centre (NPDPSC) as probable prion diseases, but which showed no biochemical or genetic evidence of prion disease after *PRNP* gene sequencing and demonstrated pathological features indistinguishable from Alzheimer's disease. In 186 cases with an identifiable disease starting date from detailed clinical records and semi-structured telephone interview of patient and/or caregiver at the time of referral, the median duration of the disease was 7.2 months (95% confidence interval 5.9–8.5 months), which was ~15-fold ($P < 0.001$) shorter than 9 years in autopsy-proven Alzheimer's disease case records ($n = 2605$) obtained from the National Alzheimer's Coordinating Centre (NACC) database at the University of Washington (Beekly *et al.*, 2007) (Fig. 1A). In all Alzheimer's disease cases, the Illumina and Sanger Sequencing of *APP* and *PSEN2* genes identified no novel rare variants or known mutations when compared to the reference Alzheimer Disease and Frontotemporal Dementia Mutation Database, and the Exome Variant Server (EVS). In 1 of 78 sequenced cases with rapidly progressive Alzheimer's disease, we identified a previously reported pathogenic mutation (M139I) in exon 5 of *PSEN1* (Kim *et al.*, 2010) and this case was excluded from the rapidly progressive Alzheimer's disease cohort analysis. Next, we excluded cases for which no frozen tissue was available as well as all cases with either an autosomal dominant pattern of the familial form of dementia or pathological features independently associated with cognitive decline (e.g. Lewy bodies, vascular brain injury, or hippocampal sclerosis) and randomly selected 30 cases according to criteria described in detail in the 'Materials and methods' section (Table 1). The demographic data distributions, characterized by sample means or proportions, did not significantly differ from all NPDPSC cases and were within the range of cases with rapidly progressive Alzheimer's disease published by European and Japanese prion centres (Schmidt *et al.*, 2012).

Our second cohort consisted of classical Alzheimer's disease cases with progression rates and demographics matching the distribution in the NACC data set that were collected at the Case Western Reserve University (CWRU) Memory and Aging Centre (see 'Materials and methods' section), and hereafter referred to as slowly progressive Alzheimer's disease (Table 1). The low frequency of *APOE* gene e4 allele in our rapidly progressive Alzheimer's disease ($n = 26$) cohort at the NPDPSC (Fig. 1B and Table 1) agrees with findings from prion centres in Japan and Europe (Schmidt *et al.*, 2011). Neuropathological evaluation according to the National Institutes of Aging – Alzheimer's Association guidelines (Montine *et al.*, 2012) suggested a trend toward more cases with less severe pathology in the rapidly progressive Alzheimer's disease group but the difference was not statistically significant (Fig 1C and D). We also found no differentiating patterns in the morphology of neurofibrillary tangles and amyloid plaques, or their distribution in different anatomical areas. As illustrated in Supplementary Fig. 1, we did not observe α-synuclein deposits or TDP-43 (now known as TARDBP) proteinopathy that could explain the difference in progression rate by comorbid pathology. Additionally, the diffuse and glial deposits of amyloid-β (Akiyama *et al.*, 1999) occur inconsistently in both rapidly progressive and slowly progressive Alzheimer's disease cases, and if present, constituted a very small proportion of the total amyloid-β deposition (Supplementary Fig. 1). Cumulatively, the consistent very rapid progression rate, genetic, and neuropathological findings of rapidly progressive Alzheimer's disease in prion centres across various methodologies, populations, and healthcare systems is evidence for a distinct especially malignant form of sporadic Alzheimer's disease, associated with a low frequency of e4 allele of the *APOE* gene that is similar to the general population.

The primary goal of the study was to establish conformational structural characteristics of amyloid-β in neuropathologically verified rapidly and slowly progressive Alzheimer's disease and thus correlation of clinical phenotypes beyond clearly defined disease duration is limited by both small group size and availability of medical records. Nonetheless, we observed a trend toward fewer cases with cognitive symptomatology in the rapidly progressive Alzheimer's disease cohort at the time of diagnosis when both groups already shared a similar frequency of other neurological and behavioural symptoms (Supplementary Table 1). This asymmetry of cognitive symptomatology, together with rapid progression, is likely responsible for the clinical conclusion of probable prion disease and referrals of rapidly progressive Alzheimer's disease patients to Prion Centres. However, the prospective longitudinal studies of rapidly progressive Alzheimer's disease with similarly assessed controls are needed to determine the detailed neurological endophenotypic differences between the groups, as well as external cofactors that may be associated with rapid progression.

Domain display and distribution of amyloid-β_{42} and amyloid-β_{40} in rapidly progressive and slowly progressive Alzheimer's disease

To investigate levels and conformational characteristics of amyloid-β, we adopted an AlphaLISA-formatted CDI (Supplementary Fig. 2A) (Safar *et al.*, 1998; Kim *et al.*, 2011, 2012; Haldiman *et al.*, 2013). This extremely sensitive assay played a critical role in discovering that a

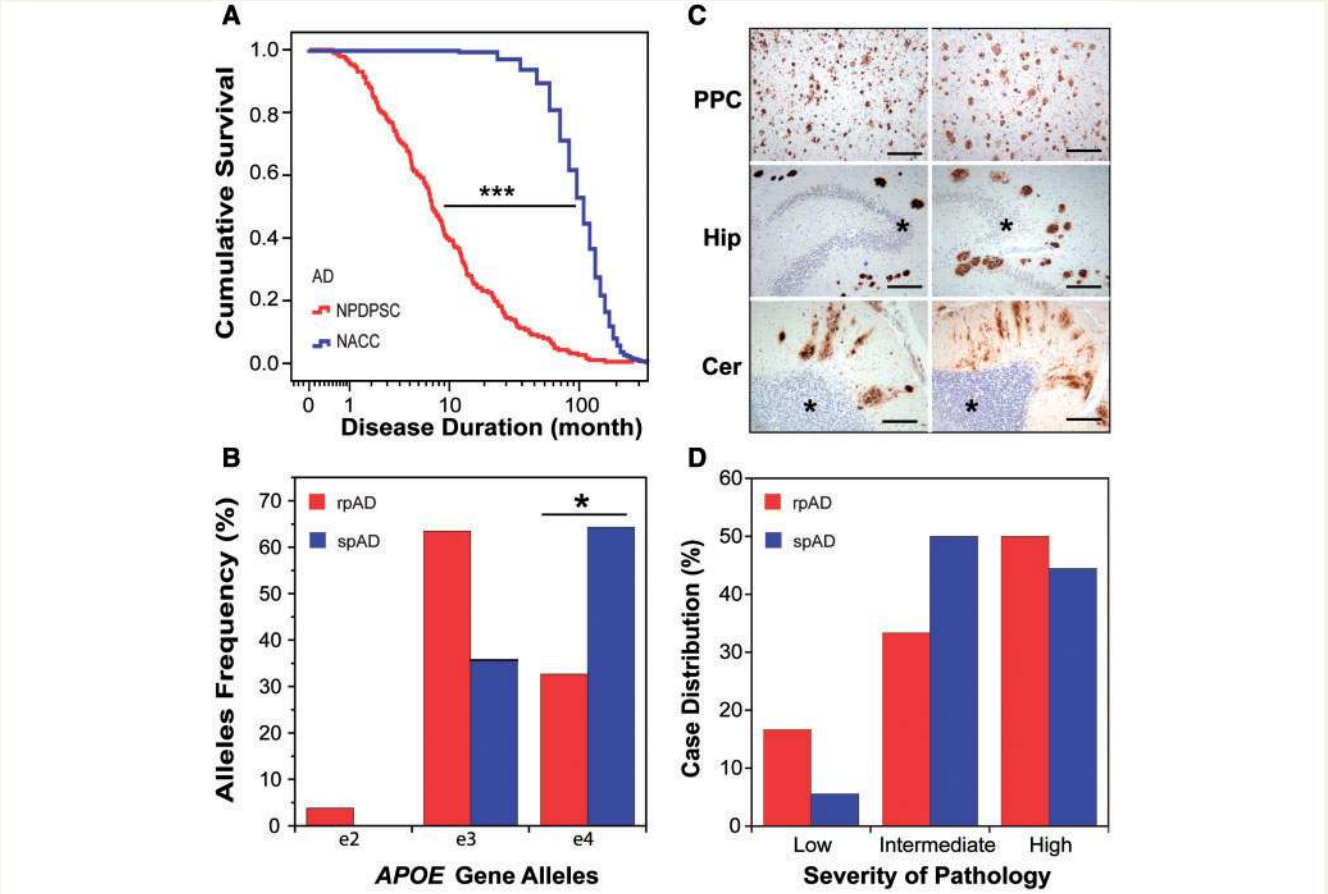

Figure 1 Rapid rates of progression in Alzheimer's disease are linked to low frequency of e4 allele in *APOE* gene but the end-point extent of amyloid or neurofibrillary tangles deposits is similar. (**A**) Kaplan-Meier cumulative survival analysis of cases with pathologically verified Alzheimer's disease (AD) that were initially referred to National Prion Disease Pathology Surveillance Centre (NPDPSC) with rapidly progressive dementia ($n = 186$) and cases of Alzheimer's disease ($n = 2605$) collected at National Alzheimer's Coordinating Centre (NACC) database at University of Washington (Beekly *et al.*, 2007). Statistical significance for difference in survival at $^{***}P < 0.001$ was determined with the log rank (Mantel-Cox) and generalized Wilcoxon test. (**B**) Frequency of e4 allele of *APOE* gene allelic polymorphisms in rapidly ($n = 26$) and slowly ($n = 18$) progressive cases of Alzheimer's disease. Statistical significance at $^{*}P < 0.05$ was determined with two-tailed Fisher's exact test. (**C**) Typical sections of precuneus/posterior cingulate cortex (PPC), hippocampus (Hip), and cerebellum (Cer) from patients with rapidly (*left*) and slowly progressive Alzheimer's disease (*right*). Immunohistochemistry was performed with anti-amyloid-β monoclonal antibody (BAM-10). Granule neurons of the dentate gyrus (Hip) and cerebellar granular cell layer (Cer) are designated by asterisk. Internal scale bars = 100 μm. (**D**) Severity of pathology classified according National Institute on Aging – Alzheimer's Association guidelines for the neuropathologic assessment (Montine *et al.*, 2012) in rapidly ($n = 24$) and slowly ($n = 18$) progressive cases of Alzheimer's disease. rpAD = rapidly progressing Alzheimer's disease; spAD = slowly progressing Alzheimer's disease.

variable proportion of pathogenic prion protein is composed of small protease-sensitive oligomers, and also helped to establish that the conformation of pathogenic prion protein varies between distinct strains of prions (Safar *et al.*, 1998; Kim *et al.*, 2011, 2012; Haldiman *et al.*, 2013). In principle, we adopted the AlphaLISA design with one antibody specific to the N-terminus (mAb 82E1, epitope amyloid-$\beta_{10\text{-}17}$) and a second antibody specific either to the C-terminus of amyloid-β_{42} (mAb12F4) or amyloid-β_{40}. The luminescence signal is generated only when the donor and acceptor beads are brought together in close proximity by simultaneous capture of N- and C-terminus of amyloid-β. Measurements performed before and after denaturation with 7 M Gdn HCl at 80°C, expressed as a denatured/native signal (D/N), allow quantitation of the exposure of both domains in the native state, thereby enabling direct comparison of global assembly structures in different brain samples without requiring prior purification (Safar *et al.*, 1998, 2002; Safar, 2012*a*, *b*; Prusiner *et al.*, 2004; Kim *et al.*, 2011, 2012). The initial experiments with age-matched sporadic Creutzfeldt-Jakob disease (CJD) and Alzheimer's disease brains demonstrated high sensitivity and conformational specificity of D/N ratio for amyloid-β_{42} present in Alzheimer's disease brains (Supplementary Fig. 3A and B). The conformational sensitivity and relative independence of the D/N ratio on amyloid-β_{42} concentration in Alzheimer's disease is shown in Supplementary Fig. 3C.

Table 1 Demographics and descriptive statistics of patients with rapidly progressive Alzheimer's disease (n = 30) and slowly progressive Alzheimer's disease (n = 18)

			Rapidly progressive Alzheimer's disease				Signif	Slowly progressive Alzheimer's disease			
Parameter		**Unit**	***n***	**Min**	**Max**	**Mean±SEM**	***P***	***n***	**Min**	**Max**	**Mean±SEM**
Sex		F/M	15/15				NS	14/4			
Age		years	30	44.0	87.0	60.0 ± 1.6	<0.001	18	61	101	82 ± 2.8
Education		years	8	11	16	13.1 ± 2.0	NS	18	11	20	13.6 ± 3.3
APOE	***e2***	*n* (%)	2 (3.8)				NS	0 (0)			
allele	***e3***	*n* (%)	33 (63.5)				NS	10 (35.7)			
frequency	***e4***	*n* (%)	17 (32.7)				0.02	18 (64.3)			
Disease duration	**From neurol. follow-up**	month	20	0.8	36.0	11.6 ± 1.7	<0.001	18	60.0	168.0	81.6 ± 8.0
Amyloid-β_{42}	**PPC**	ng/ml	26	128.0	1598.3	790.3 ± 67.9	0.030	18	306.9	1216.3	560.1 ± 71.7
		D/N ratio	26	5.8	38.5	16.0 ± 1.5	0.017	18	7.3	52.3	23.5 ± 3.5
	Hippocampus	ng/ml	26	97.2	1675.2	481.6 ± 74.4	NS	18	201.0	1155.8	476.3 ± 60.7
		D/N ratio	26	3.1	28.3	12.1 ± 1.2	0.004	18	5.8	40.3	19.2 ± 2.3
	Cerebellum	ng/ml	30	6.5	1239.1	136.8 ± 45.0	NS	18	7.9	457.0	149.6 ± 43.4
		D/N ratio	30	0.9	20.0	4.7 ± 1.0	NS	18	1.3	24.2	8.7 ± 2.2
Amyloid-β_{40}	**PPC**	ng/ml	13	4.3	54.7	19.2 ± 3.5	NS	7	2.8	421.2	78.3 ± 41.0
		D/N ratio	13	0.8	11.2	3.3 ± 0.7	NS	7	0.7	17.7	5.5 ± 1.8
	Hippocampus	ng/ml	13	3.8	199.3	29.4 ± 10.3	NS	7	3.6	53.6	20.0 ± 4.6
		D/N ratio	13	0.7	15.1	3.2 ± 0.8	NS	7	1.0	7.8	3.0 ± 0.6
	Cerebellum	ng/ml	15	4.0	85.1	19.5 ± 4.8	NS	7	2.9	133.1	29.2 ± 12.8
		D/N ratio	15	0.7	30.1	5.5 ± 1.7	NS	7	1.0	15.0	3.5 ± 1.4

Compared with slowly progressive Alzheimer's disease, the cases of rapidly progressive Alzheimer's disease accumulated more amyloid-β_{42} in the precuneus/posterior cingulate cortex with significantly lower D/N ratios in both cingulate cortex and hippocampus (Fig. 2A and B and Table 1). In contrast, the concentration of amyloid-β_{40} was invariably low in all areas in all cases (Fig. 2B), and the D/N ratio close to 2 suggests that both N- and C termini are largely exposed in the native state (Fig. 2A and Table 1). This trend toward low D/N ratios was observed in age-matched controls but in these cases for both amyloid-β_{42} and amyloid-β_{40} (Fig 2A and B, and Supplementary Table 2). Taken together, these data indicate that rapidly progressive Alzheimer's disease is associated with higher levels of amyloid-β_{42} in the posterior cingulate cortex. The amyloid-β_{42} present in both the posterior cingulate cortex and hippocampus of rapidly progressive Alzheimer's disease formed either (i) smaller particles; (ii) particles with a differently exposed N- and C-termini of amyloid-β_{42} due to the distinct conformation; or (iii) both. The data obtained in age-matched non-Alzheimer's disease controls including sporadic CJD indicate that these aspects are not a simple result of ageing.

Conformational stability of amyloid-β_{42} in rapidly progressive and slowly progressive Alzheimer's disease

To investigate whether observed variations in exposed N- and C-terminal domains of amyloid-β_{42} in rapidly progressive Alzheimer's disease are due to conformational differences, we employed a conformational stability assay (Supplementary Fig. 2B) (Safar and Prusiner, 1998). Even relatively small variations in protein structure can be determined by measuring conformational stability in a denaturant such as Gdn HCl (Shirley, 1995). Based on this concept, we designed a procedure in which misfolded protein in brain tissue is first exposed to the denaturant Gdn HCl, and then exposed to monoclonal antibody against epitopes that are hidden in the native conformation (Safar and Prusiner, 1998). As the concentration of Gdn HCl increases, the amyloid form of the protein unfolds and the epitopes become available to antibody binding. The Gdn HCl value found at the half-maximal denaturation ($[\text{Gdn HCl}]_{1/2}$) was used as a measure of the relative conformational stability of a protein. If the compared proteins have the same amino acid sequence, then the differences in stability are evidence of different conformations (Shirley, 1995; Safar *et al.*, 1998; Safar, 2012*a*, *b*).

Cumulative plots of unfolding curves were obtained for amyloid-β_{42} present in brain homogenates that were prepared from hippocampi of patients with rapidly progressive Alzheimer's disease (n = 10) and slowly progressive Alzheimer's disease (n = 10) (Fig 3A and B); these plots indicate a remarkable variability of amyloid-β_{42} unfolding, and instead of the expected simple biphasic transition from native to denatured state, the plots display curves with up to three stages of unfolding in all Alzheimer's disease cases. Each of these stages represents amyloid-β_{42} with increasing resistance to denaturant; the least populated and the least stable amyloid-β_{42} conformers unfold between 2.5 and

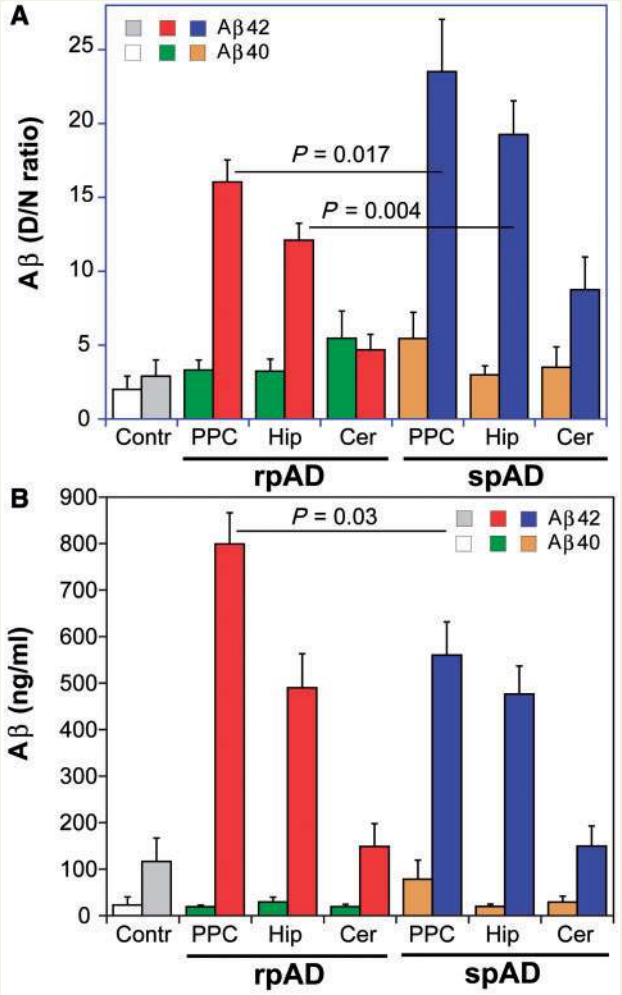

Figure 2 The cases with rapidly progressive Alzheimer's disease accumulate amyloid-β_{42} structures with more exposed N- and C-terminal domains in cingulate and hippocampal cortex. (**A**) The D/N ratio was calculated from the AlphaLISA signal before (native, N) and after denaturation (denatured, D) of amyloid-β_{42} and amyloid-β_{40} in precuneus/posterior cingulate cortex (PPC), hippocampus (Hip), and cerebellum (Cer) of rapidly progressive Alzheimer's disease (n = 26) and slowly progressive Alzheimer's disease (n = 18) cases. The cases in which neuropathologic assessment ruled out Alzheimer's disease, prion, or other neurodegenerative diseases were used as age-matched non-Alzheimer's disease controls (Contr) (n = 8). The denatured state is a reference and the lower ratio indicates more exposed N- and C-terminal epitopes in native structures due to the smaller particles, different conformation, or both (Safar *et al.*, 1998; Kim *et al.*, 2011, 2012). (**B**) The levels of amyloid-β_{42} and amyloid-β_{40} in 10% homogenate of the parietal posterior cingulate cortex (PPC), hippocampus (Hip), and cerebellum (Cer) were obtained from samples denatured with 7 M Gdn HCl at 80°C. Each sample was measured in triplicate and the concentration was determined by AlphaLISA-formatted CDI calibrated with synthetic amyloid-β peptides. The bars are mean ± SEM for each parameter and statistical significance was determined with ANOVA. rpAD = rapidly progressing Alzheimer's disease; spAD = slowly progressing Alzheimer's disease.

4.5 M of Gdn HCl and the second more abundant population of conformers unfolds between 4.5 and 6 M of Gdn HCl. Interestingly, the third pool of amyloid-β_{42} conformers is remarkably resistant to denaturation, and in some samples, a variable fraction of amyloid-β_{42} did not complete unfolding even in 7 M of Gdn HCl at 80°C. These differences indicated up to three distinct populations of conformers in each individual sample. Although the amyloid-β_{42} accumulated in the cortex of rapidly progressive Alzheimer's disease cases is conformationally heterogeneous, the averaged data and differential curves show a statistically significant difference from slowly progressive Alzheimer's disease at 5.5 M Gdn HCl (Fig. 3C) using a mixed model analysis of the unfolding curves across all Gdn HCI levels in rapidly progressive and slowly progressive Alzheimer's disease groups (P = 0.02). Moreover, sequential ANOVA comparing the values in each group at different Gdn HCl concentrations showed the same trend (P = 0.015) and the levels of these conformers in all rapidly progressive and slowly progressive Alzheimer's disease cases correlate inversely with the disease duration in non-linear regression analysis (Fig. 3D). Cumulatively, these findings indicate that (i) a remarkably wide spectrum of amyloid-β_{42} structures exist in different cases of Alzheimer's disease; (ii) that they group into three distinct sets of conformers present in different proportions in each Alzheimer's disease case; and (iii) that amyloid-β_{42} in rapidly progressive Alzheimer's disease is conformationally more heterogeneous than in slowly progressive Alzheimer's disease with significantly higher levels of conformers with intermediate stability that unfold at ~5.5 M Gdn HCl.

The size and composition of native amyloid-β particles present in rapidly progressive and slowly progressive Alzheimer's disease

To measure the relative levels of specific particles (assemblies) of native (non-denatured) amyloid-β_{42} and amyloid-β_{40} present in brain tissue, we separated the brain samples homogenized in the non-denaturing detergent Sarkosyl, with velocity sedimentation in sucrose gradients using high-speed centrifugation. Sarkosyl is a non-denaturing detergent with a low aggregation number (~2), and has been used extensively in isolation and conformational studies of native infectious prions, including prion oligomers (Caughey *et al.*, 1991; Safar *et al.*, 1993*a*, *b*, 1994; Prusiner *et al.*, 2004; Kim *et al.*, 2011, 2012). Calibration experiments with native proteins and synthetic amyloid-β_{42} indicate that Sarkosyl does not affect the expected sedimentation velocity of the monomeric, oligomeric or fibrillar assemblies prepared *in vitro* (Supplementary Fig. 4) and maintains their size and morphology as judged by atomic force microscopy (Supplementary Fig. 5). The calculated sedimentation velocity of the oligomeric assembly of

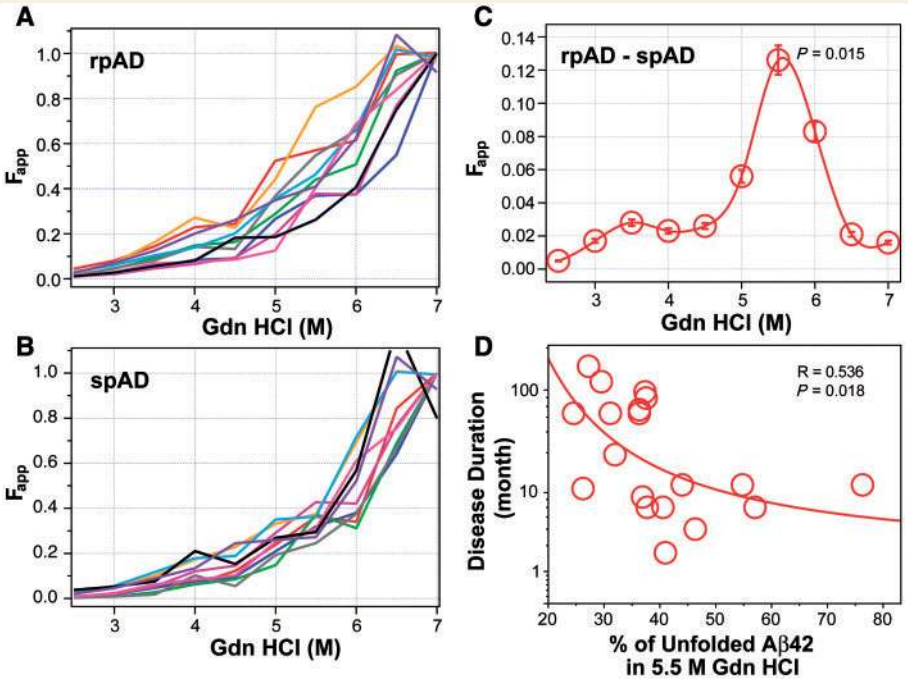

Figure 3 Structural heterogeneity and conformationally distinct subpopulations of amyloid-β_{42}. Structural heterogeneity and conformationally distinct subpopulations of amyloid-β_{42} in hippocampus of Alzheimer's disease determined directly in the brain tissue homogenate with conformational stability assay (Safar *et al.*, 1998; Kim *et al.*, 2011, 2012; Safar, 2012*a*, *b*). (**A**) Conformational stability curves of hippocampal amyloid-β_{42} in rapidly progressive Alzheimer's disease (n = 10), each curve representing dissociation and unfolding of amyloid-β_{42} in individual patients; (**B**) conformational stability curves of hippocampal amyloid-β_{42} of individual cases with slowly progressive Alzheimer's disease (n = 10); (**C**) differential stability curves of hippocampal amyloid-β_{42} in rapidly progressive and slowly progressive Alzheimer's disease fitted with Gaussian model. (**D**) The higher levels of unstable hippocampal amyloid-β_{42} conformers that are unfolding at 5.5 M Gdn HCl correlate with rapid progression of Alzheimer's disease. The values of apparent fractional change (Fapp) of each brain sample from native to denatured state are mean ± SEM obtained from triplicate measurements at each concentration of denaturant (Gdn HCl). The analysis was performed with non-linear regression and the statistical significance was determined with ANOVA. rpAD = rapidly progressing Alzheimer's disease; spAD = slowly progressing Alzheimer's disease.

synthetic amyloid-β_{42} indicated an average 50 monomers, which is expected for the dimethyl sulphoxide oligomer protocol from size-exclusion chromatography experiments (LeVine, 2004; Stine *et al.*, 2011).

We identified three major peaks in the sedimentation velocity profiles of total brain cortex followed by CDI, indicating three major populations of amyloid-β_{42} particles in Alzheimer's disease: floating, intermediate, and rapidly sedimenting fractions (Fig. 4B and C). Based on the $s\omega^2t$ value and calibration with standard proteins, we estimate that the floating fraction was composed of 1–32 monomers of amyloid-β_{42}, the intermediate of 32–750 monomers, and the rapidly sedimenting fraction of $>$ 3000 monomers of amyloid-β_{42} (Fig. 4A). Although the sizes of the particles found in the floating and intermediate oligomer fractions of amyloid-β_{42} in rapidly progressive and slowly progressive Alzheimer's disease cases were the same, the markedly low D/N ratios in rapidly progressive Alzheimer's disease are evidence for differently exposed N- and C-terminal domains, and thus indicate the presence of differing conformation (Fig. 4B). In contrast, the sedimentation velocity profiles of amyloid-β_{40} investigated in the same rapidly progressive and slowly progressive Alzheimer's disease samples showed a D/N ratio close to 2 throughout the entire sucrose gradient in all cases (Fig. 4D and E). In the posterior cingulate cortex and hippocampus, the rapidly progressive Alzheimer's disease cases accumulated lower levels of floating amyloid-β_{42} assemblies, and more particles composed of 30–130 monomers of amyloid-β_{42} (Fig. 4C). In marked distinction, the brain amyloid-β_{40} demonstrated no evidence of a major particle pool. The age-matched non-Alzheimer's disease cases showed low D/N ratio through the whole gradient for both amyloid-β_{42} and amyloid-β_{40} and no evidence of formation of distinct particle composed of amyloid-β_{42} or amyloid-β_{40} (Fig. 4H and I). We conclude from these experiments that amyloid-β_{40}: (i) exists with largely exposed N- and C-terminal domains; (ii) does not participate in assemblies of amyloid-β_{42}; and (iii) does not form a discernible major particle population. Furthermore, the cases with rapidly progressive Alzheimer's disease accumulated lower levels of particles composed of $\leqslant$ 30 monomers and higher levels of amyloid-β_{42} particles composed of 30–100 monomers in the posterior cingulate cortex and hippocampus. These assemblies demonstrated differently exposed N- and C-termini than those of the same size present in the cases with slowly progressive Alzheimer's disease. We concluded that these particles have different conformational

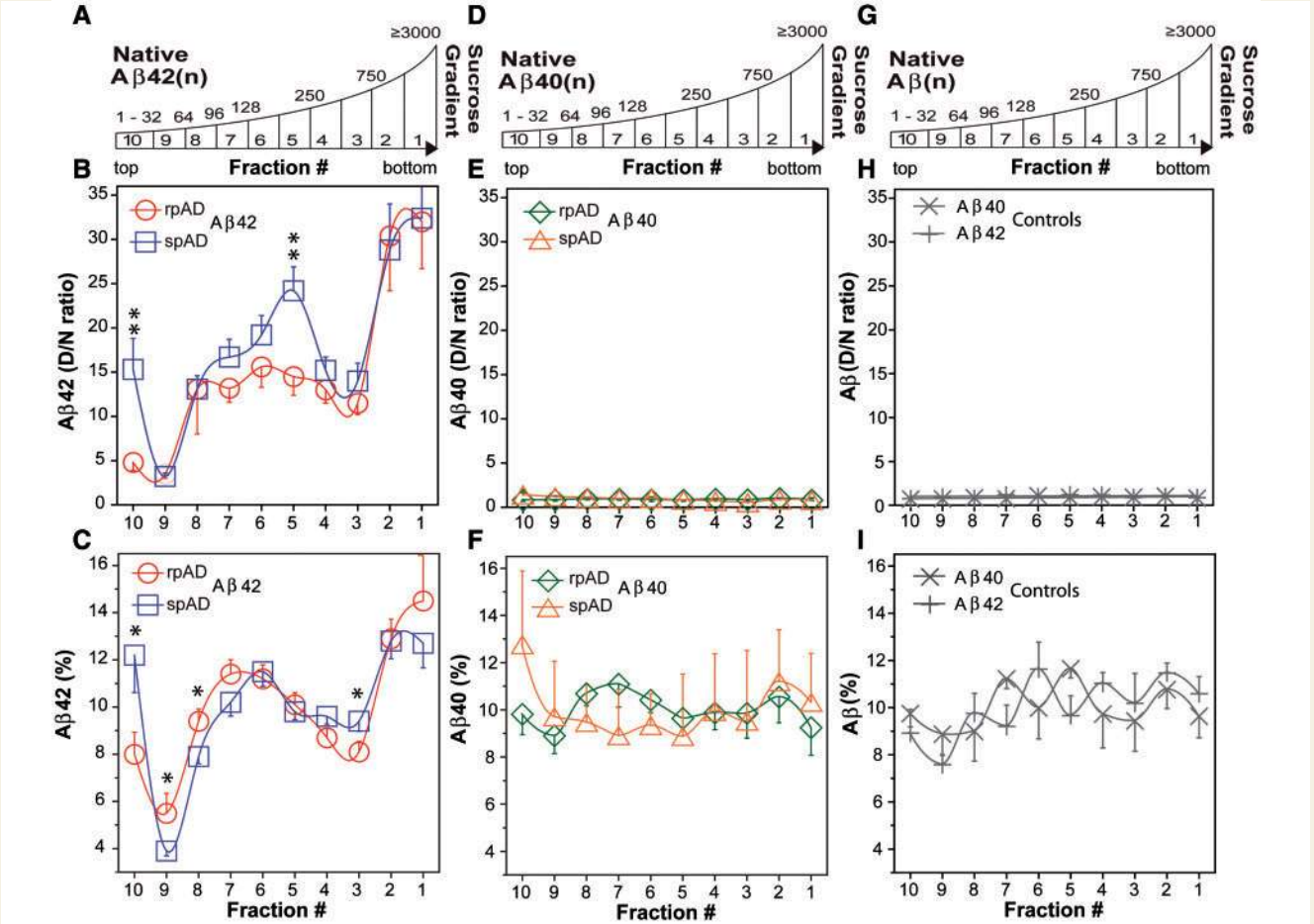

Figure 4 Particles of different sizes composed of amyloid-β_{42} but not amyloid-β_{40} in the hippocampal cortex of rapidly progressive Alzheimer's disease (n = 10), slowly progressive Alzheimer's disease (n = 10), and age-matched non-Alzheimer's disease controls (n = 4). The samples were fractionated by sedimentation velocity using ultracentrifugation in sucrose gradient and analysed by CDI-formatted AlphaLISA. (**A**, **D** and **G**) Schematic representation of sedimentation velocity profile in sucrose gradient calibrated with standard proteins and synthetic amyloid-β_{42} in monomeric, oligomeric, and fibrillar state (Supplementary Fig. 3). (**B**, **E** and **H**) Exposure of N- and C-terminal domains in distinct particle assemblies of amyloid-β_{42} and amyloid-β_{40} monitored with D/N ratio in rapidly progressive Alzheimer's disease (n = 10), slowly progressive Alzheimer's disease (n = 10), and age-matched controls (n = 4). (**C**, **F** and **I**) Relative distribution of particles of amyloid-β_{42} and amyloid-β_{40} according to sedimentation velocity in calibrated sucrose gradient. The CDI was performed in duplicate or triplicate for each sucrose fraction of each Alzheimer's disease case sample and the points and bars are average ± SEM. Statistical significance at $^{*}P < 0.05$ and $^{**}P < 0.01$ was determined with ANOVA. rpAD = rapidly progressing Alzheimer's disease; spAD = slowly progressing Alzheimer's disease.

structures in rapidly progressive than in slowly progressive Alzheimer's disease. These aspects are not a simple result of ageing as evidenced with the data obtained from age-matched non-Alzheimer's disease controls.

To investigate the composition of the complete pool of amyloid-β particles present in the brain, we performed gradient SDS PAGE and western blots on fractions separated by sedimentation velocity. A uniform ladder of bands of amyloid-β ranging from 4.5 kDa to 55 kDa was observed at different levels in all sucrose gradient fractions. This indicates that SDS had partially dissociated and denatured these native particles of different sizes and structures, and sorted them on SDS PAGE into similar mixtures of monomers and oligomers (Fig. 5 and Supplementary Fig. 6). Nevertheless, in rapidly progressive Alzheimer's disease cases densitometry demonstrated a higher proportion of amyloid-β oligomers in the sucrose gradient fractions with low sedimentation velocity. Cumulatively, even though western blots generally have lower sensitivity and a more narrow dynamic detection range than AlphaLISA-formatted CDI, the data showed higher levels of oligomeric amyloid-β particles in cases with rapidly progressive Alzheimer's disease and thus confirmed the results from previous CDI experiments.

Discussion

Two unsettled factors for sporadic Alzheimer's disease are: (i) the extensive variability of progression rates and phenotypes (Wilkosz *et al.*, 2010; Schmidt *et al.*, 2011); and (ii)

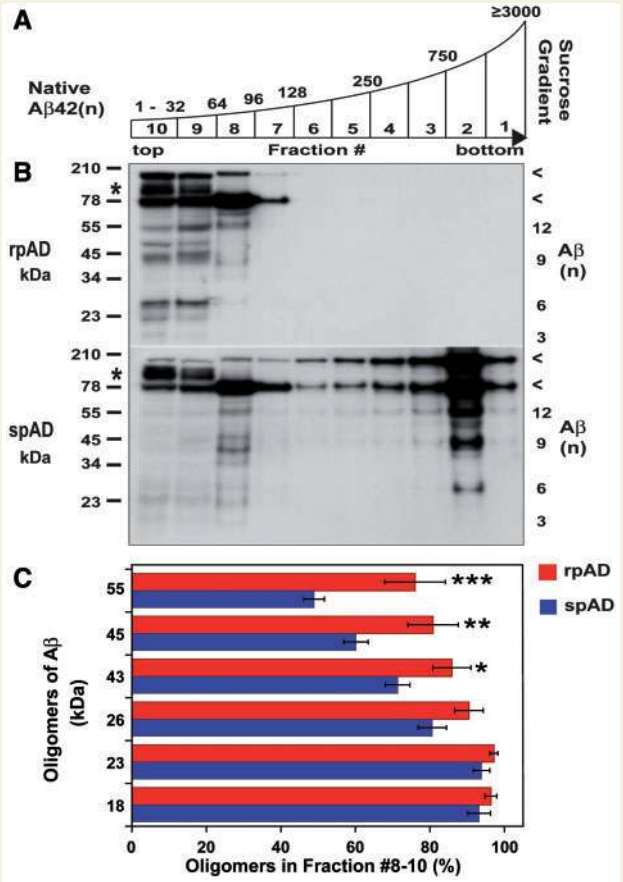

Figure 5 Preponderance of amyloid-β oligomeric species in rapidly progressive Alzheimer's disease. The comparative western blots of sucrose gradient fractions from hippocampus and precuneus/posterior cingulate cortex in rapidly progressive Alzheimer's disease (n = 12) and slowly progressive Alzheimer's disease (n = 12). (**A** and **B**) Calibration and typical western blot of sucrose gradient fractions of rapidly progressive and slowly progressive Alzheimer's disease cases with biotinylated mAb 6E10. The asterisk indicates floating APP100; arrows (<) point to the bands of a proteins cross-reacting with streptavidin-peroxidase complex. (**C**) The relative proportion of major bands of amyloid-β oligomers in top three floating fractions (#10-8) were compared with total density of a given band in all fractions from hippocampus and precuneus/posterior cingulate cortex in western blots of rapidly progressive Alzheimer's disease (n = 12) and slowly progressive Alzheimer's disease (n = 12). The densitometry was performed with ImageJ software and the bars represent cumulative average ± SEM for each band; the molecular mass of the markers is in kDa. Statistical significance at $^{*}P < 0.05$, $^{**}P < 0.01$, and $^{***}P < 0.001$ was determined with ANOVA. rpAD = rapidly progressing Alzheimer's disease; spAD = slowly progressing Alzheimer's disease.

discrepancies between amyloid-β deposit levels and clinical disease severity (Masters and Selkoe, 2012). However, using novel biophysical techniques to inventory the structural species of amyloid-β in the brain, we have defined a new variable in Alzheimer's disease pathogenesis; namely, a broad spectrum of amyloid-β_{42} particles that have distinct conformational characteristics. Remarkably, the link to disease duration did not emanate from the levels of different amyloid-β_{42} particles *per se*, but from their distinct conformations.

The conformational heterogeneity of brain amyloid-β_{42} that we uncovered in sporadic Alzheimer's disease is striking, and implies the presence of numerous distinct structures that may have very different toxicity and propagation rates in the pathogenesis of Alzheimer's disease. Although disease-causing mutations in the amyloid-β precursor and its processing genes have indisputably established the central role of amyloid-β in the pathogenesis of early onset Alzheimer's disease, the loose correlations between amyloid plaque load and severity of sporadic Alzheimer's disease (Masters and Selkoe, 2012) have generated a pathogenetic conundrum (Colom *et al.*, 2013). Consequently, these discrepancies, and the structural plasticity of synthetic amyloid-β peptide observed *in vitro*, has pointed to the need to improve our understanding of the structure of amyloid-β in brain tissue. To fill this void, we elected to determine the domain display and the stability of amyloid-β using sandwich CDI (Safar *et al.*, 1998), which allows us to compare different conformational structures formed by the same protein or peptide. If these structures have the same amino acid sequence, then the difference in the domain display and the susceptibility to denaturation (stability) is a reliable indicator of a distinct native conformation in brain tissue (Shirley, 1995; Safar *et al.*, 1998). This technique has been extensively validated and is used in prion laboratories worldwide (Peretz *et al.*, 2002; Colby *et al.*, 2010; Choi *et al.*, 2011*a*, *b*; Pirisinu *et al.*, 2011). Determining stability using the sandwich CDI allows us to compare the global stability of a protein directly in brain tissue over a concentration range of five orders of magnitude, with sensitivity ~4 pg/ml; as a result, the procedure yields highly reproducible curves that differentiate various prion conformers, which originate from distinct strains of prions (Safar *et al.*, 1998; Safar, 2012*a*, *b*).

Surprisingly, we found evidence of up to three populations of amyloid-β_{42} conformers with varying structures. Despite the extensive conformational variability of amyloid-β_{42} in rapidly progressive Alzheimer's disease, we found a common pattern of significantly more conformers that were less stable and unfolded at 3.5 and 5.5 M of denaturant (Fig. 3). The lower stability of these amyloid-β_{42} structures suggests that they may be more susceptible to dissociation *in vivo*, in contrast to the more abundant and very stable conformers at ⩾ 7M Gdn HCl. In prions, lower stability correlates with easier fragmentation, which is responsible for faster replication, and more rapid progression of disease (Kim *et al.*, 2011, 2012). Even though the extraordinary structural diversity of amyloid-β_{42} in rapidly progressive Alzheimer's disease far exceeds the structural heterogeneity of human prions (Kim *et al.*, 2011, 2012), whether this fundamental paradigm applies to amyloid-β_{42} in Alzheimer's disease has yet to be investigated.

Previous studies posit a toxic subform of amyloid-β to explain the discrepancy between amyloid load and the onset of clinical symptoms in Alzheimer's disease (Masters and Selkoe, 2012; Lesne *et al.*, 2013). But there is an ongoing debate if, and which, of the toxic oligomers observed *in vitro* exist in the brains of patients with Alzheimer's disease, and what role they play in the Alzheimer's disease pathogenesis (Benilova *et al.*, 2012; Hayden and Teplow, 2013). Our experiments provide direct evidence for a broad spectrum of amyloid-β_{42} particles in the Alzheimer's disease brain, which group into three major peaks, composed of ~30, ~100, and > 3000 monomers. The differently exposed N- and C-terminal domains of amyloid-β_{42} in these native particles suggest that different size particles represent distinct structures. In marked contrast, amyloid-β_{40} did not form a major particle of discernible size, did not participate in the formation of the major amyloid-β_{42} particles, and appears to exist mostly as a uniform monomeric peptide. In both rapidly progressive and slowly progressive Alzheimer's disease, amyloid-β_{42} particles composed of > 3000 monomers shared similar levels and domain displays. However, rapidly progressive Alzheimer's disease cases accumulated fewer ~30-mers and more ~100-mers, with more exposed N- and C-terminal domains in the native state than slowly progressive Alzheimer's disease cases. We also demonstrated that even identically sized particles may have different conformations. Thus far, we have not yet identified whether these differences are due to the structure of the monomeric building block or the way the monomers are assembled (quaternary structure), but the prevailing view is that both these aspects must be thermodynamically and kinetically linked (Tycko, 2006; Paravastu *et al.*, 2008).

Cumulatively, our data demonstrate that different rates of clinical decline in Alzheimer's disease are linked to different polymorphisms in the *APOE* gene, and distinct conformational characteristics of the amyloid-β_{42}. To determine whether additional external disease modifiers, such as early life environment, education, occupation, and toxic exposures contribute to the rapidly progressive Alzheimer's disease endophenotype will require prospective longitudinal clinical follow-up. For example, educational attainment has been linked to progression rates in amnestic mild cognitive impairment (MCI), likely through a cognitive reserve mechanism (Amieva *et al.*, 2014); but this effect on disease progression disappears after the onset of dementia (Ye *et al.*, 2013; Amieva *et al.*, 2014). Thus, our findings infer the paradigm that emerged recently in investigations of human prion diseases where the synergy between polymorphisms in the prion protein gene (*PRNP*) and variable conformational characteristics of the pathogenic prion protein leads to vastly different disease phenotypes (Puoti *et al.*, 2012; Safar, 2012*a*, *b*). To address this possibility in Alzheimer's disease will require analysing prospectively detailed endophenotypic characteristics, identifying polymorphisms in genes that may be contributing to the Alzheimer's disease phenotype, in parallel with establishing detailed characteristics of different conformational subsets of brain amyloid-β_{42}.

Acknowledgements

The authors are grateful to the patient's families, the CJD Foundation, all the members of the National Prion Disease Pathology Surveillance Centre for their help and review of clinical data. The authors would like to thank the NHLBI GO Exome Sequencing Project and its ongoing studies which produced and provided exome variant calls for comparison: the Lung GO Sequencing Project (HL-102923), the WHI Sequencing Project (HL-102924), the Broad GO Sequencing Project (HL-102925), the Seattle GO Sequencing Project (HL-102926) and the Heart GO Sequencing Project (HL-103010).

Funding

The NACC database is funded by NIA Grant U01 AG016976 and this work was supported by grants from NINDS (NS074317), CDC (UR8/CCU515004), and the Spitz Foundation.

Supplementary material

Supplementary material is available at *Brain* online.

References

Akiyama H, Mori H, Saido T, Kondo H, Ikeda K, McGeer PL. Occurrence of the diffuse amyloid beta-protein (Abeta) deposits with numerous Abeta-containing glial cells in the cerebral cortex of patients with Alzheimer's disease. Glia 1999; 25: 324–31.

Amieva H, Mokri H, Le Goff M, Meillon C, Jacqmin-Gadda H, Foubert-Samier A, et al. Compensatory mechanisms in higher-educated subjects with Alzheimer's disease: a study of 20 years of cognitive decline. Brain 2014; 137 (Pt 4): 1167–75.

Beekly DL, Ramos EM, Lee WW, Deitrich WD, Jacka ME, Wu J, et al. The National Alzheimer's Coordinating Center (NACC) database: the Uniform Data Set. Alzheimer Dis Assoc Disord 2007; 21: 249–58.

Bellon A, Seyfert-Brandt W, Lang W, Baron H, Groner A, Vey M. Improved conformation-dependent immunoassay: suitability for human prion detection with enhanced sensitivity. J Gen Virol 2003; 84: 1921–5.

Benilova I, Karran E, De Strooper B. The toxic Abeta oligomer and Alzheimer's disease: an emperor in need of clothes. Nat Neurosci 2012; 15: 349–57.

Braak H, Del Tredici K. Evolutional aspects of Alzheimer's disease pathogenesis. J Alzheimers Dis 2013; 33 (Suppl 1): S155–61.

Caughey BW, Dong A, Bhat KS, Ernst D, Hayes SF, Caughey WS. Secondary structure analysis of the scrapie-associated protein PrP 27-30 in water by infrared spectroscopy. Biochemistry 1991; 30: 7672–80.

Chien DT, Szardenings AK, Bahri S, Walsh JC, Mu F, Xia C, et al. Early clinical PET imaging results with the novel PHF-tau radioligand [F18]-T808. J Alzheimers Dis 2014; 38: 171–84.

Chitravas N, Jung RS, Kofskey DM, Blevins JE, Gambetti P, Leigh RJ, et al. Treatable neurological disorders misdiagnosed as Creutzfeldt-Jakob disease. Ann Neurol 2011; 70: 437–44.

Choi YP, Groner A, Ironside JW, Head MW. Comparison of the level, distribution and form of disease-associated prion protein in variant and sporadic Creutzfeldt-Jakob diseased brain using conformation-dependent immunoassay and Western blot. J Gen Virol 2011a; 92 (Pt 3): 727–32.

Choi YP, Peden AH, Groner A, Ironside JW, Head MW. Distinct stability states of disease-associated human prion protein identified by conformation-dependent immunoassay. J Virol 2011b; 84: 12030–8.

Colby DW, Wain R, Baskakov IV, Legname G, Palmer CG, Nguyen HO, et al. Protease-sensitive synthetic prions. PLoS Pathog 2010; 6: e1000736.

Colom LV, Perry G, Kuljis RO. Tackling the elusive challenges relevant to conquering the 100-plus year old problem of Alzheimer's disease. Curr Alzheimer Res 2013; 10: 108–16.

Cruts M, Theuns J, Van Broeckhoven C. Locus-specific mutation databases for neurodegenerative brain diseases. Hum Mutat 2012; 33: 1340–4.

Geschwind MD, Shu H, Haman A, Sejvar JJ, Miller BL. Rapidly progressive dementia. Ann Neurol 2008; 64: 97–108.

Guo JL, Lee VM. Neurofibrillary tangle-like tau pathology induced by synthetic tau fibrils in primary neurons over-expressing mutant tau. FEBS Lett 2013; 587: 717–23.

Haldiman T, Kim C, Cohen Y, Chen W, Blevins J, Qing L, et al. Coexistence of distinct prion types enables conformational evolution of human PrPSc by competitive selection. J Biol Chem 2013; 288: 29846–61.

Hayden EY, Teplow DB. Amyloid beta-protein oligomers and Alzheimer's disease. Alzheimers Res Ther 2013; 5: 60.

Kabir ME, Safar JG. Implications of prion adaptation and evolution paradigm for human neurodegenerative diseases. Prion 2014; 8: 111–6.

Kane MD, Lipinski WJ, Callahan MJ, Bian F, Durham RA, Schwarz RD, et al. Evidence for seeding of beta-amyloid by intracerebral infusion of Alzheimer brain extracts in beta-amyloid precursor protein-transgenic mice. J Neurosci 2000; 20: 3606–11.

Kim C, Haldiman T, Cohen Y, Chen W, Blevins J, Sy MS, et al. Protease-sensitive conformers in broad spectrum of distinct PrP structures in sporadic creutzfeldt-jakob disease are indicator of progression rate. PLoS Pathog 2011; 7: e1002242.

Kim C, Haldiman T, Surewicz K, Cohen Y, Chen W, Blevins J, et al. Small protease sensitive oligomers of PrP(Sc) in distinct human prions determine conversion rate of PrP(C). PLoS Pathog 2012; 8: e1002835.

Kim HJ, Kim HY, Ki CS, Kim SH. Presenilin 1 gene mutation (M139I) in a patient with an early-onset Alzheimer's disease: clinical characteristics and genetic identification. Neurol Sci 2010; 31: 781–3.

Lesne SE, Sherman MA, Grant M, Kuskowski M, Schneider JA, Bennett DA, et al. Brain amyloid-beta oligomers in ageing and Alzheimer's disease. Brain 2013; 136 (Pt 5): 1383–98.

LeVine H III. Alzheimer's beta-peptide oligomer formation at physiologic concentrations. Anal Biochem 2004; 335: 81–90.

Masters CL, Selkoe DJ. Biochemistry of amyloid beta-protein and amyloid deposits in Alzheimer disease. Cold Spring Harb Perspect Med 2012; 2: a006262.

Mays CE, Kim C, Haldiman T, van der Merwe J, Lau A, Yang J, et al. Prion disease tempo determined by host-dependent substrate reduction. J Clin Invest 2014; 124: 847–58.

McCutcheon S, Hunter N, Houston F. Use of a new immunoassay to measure PrP Sc levels in scrapie-infected sheep brains reveals PrP genotype-specific differences. J Immunol Methods 2005; 298: 119–28.

McKhann GM, Knopman DS, Chertkow H, Hyman BT, Jack CR Jr, Kawas CH, et al. The diagnosis of dementia due to Alzheimer's disease: recommendations from the National Institute on Aging-Alzheimer's Association workgroups on diagnostic guidelines for Alzheimer's disease. Alzheimers Dement 2011; 7: 263–9.

Meyer-Luehmann M, Coomaraswamy J, Bolmont T, Kaeser S, Schaefer C, Kilger E, et al. Exogenous induction of cerebral beta-amyloidogenesis is governed by agent and host. Science 2006; 313: 1781–4.

Montine TJ, Phelps CH, Beach TG, Bigio EH, Cairns NJ, Dickson DW, et al. National Institute on Aging-Alzheimer's Association guidelines for the neuropathologic assessment of Alzheimer's disease: a practical approach. Acta Neuropathol 2012; 123: 1–11.

Paravastu AK, Leapman RD, Yau WM, Tycko R. Molecular structural basis for polymorphism in Alzheimer's beta-amyloid fibrils. Proc Natl Acad Sci USA 2008; 105: 18349–54.

Parchi P, Castellani R, Capellari S, Ghetti B, Young K, Chen SG, et al. Molecular basis of phenotypic variability in sporadic Creutzfeldt-Jakob disease. Ann Neurol 1996; 39: 767–78.

Parchi P, Zou W, Wang W, Brown P, Capellari S, Ghetti B, et al. Genetic influence on the structural variations of the abnormal prion protein. Proc Natl Acad Sci USA 2000; 97: 10168–72.

Peretz D, Williamson RA, Legname G, Matsunaga Y, Vergara J, Burton D, et al. A change in the conformation of prions accompanies the emergence of a new prion strain. Neuron 2002; 34: 921–32.

Pirisinu L, Di Bari M, Marcon S, Vaccari G, D'Agostino C, Fazzi P, et al. A new method for the characterization of strain-specific conformational stability of protease-sensitive and protease-resistant PrP. PLoS One 2011; 5: e12723.

Prusiner SB. Cell biology. A unifying role for prions in neurodegenerative diseases. Science 2012; 336: 1511–3.

Prusiner SB. Biology and genetics of prions causing neurodegeneration. Annu Rev Genet 2013; 47: 601–23.

Prusiner SB, Hadlow WJ, Eklund CM, Race RE, Cochran SP. Sedimentation characteristics of the scrapie agent from murine spleen and brain. Biochemistry 1978; 17: 4987–92.

Prusiner SB, Legname G, DeArmond SJ, Cohen FE, Safar J, Riesner D, et al. Some strategies and methods for the study of prions. In: Prusiner SB, editor. Prion Biology and diseases. 2nd edn. Cold Spring Harbor: Cold Spring Harbor Laboratory Press; 2004. p. 857–920.

Puoti G, Bizzi A, Forloni G, Safar JG, Tagliavini F, Gambetti P. Sporadic human prion diseases: molecular insights and diagnosis. Lancet Neurol 2012; 11: 618–28.

Safar J, Prusiner SB. Molecular studies of prion diseases. Prog Brain Res 1998; 117: 421–34.

Safar J, Roller PP, Gajdusek DC, Gibbs CJ Jr. Conformational transitions, dissociation, and unfolding of scrapie amyloid (prion) protein. J Biol Chem 1993a; 268: 20276–84.

Safar J, Roller PP, Gajdusek DC, Gibbs CJ Jr. Thermal stability and conformational transitions of scrapie amyloid (prion) protein correlate with infectivity. Protein Sci 1993b; 2: 2206–16.

Safar J, Roller PP, Gajdusek DC, Gibbs CJ Jr. Scrapie amyloid (prion) protein has the conformational characteristics of an aggregated molten globule folding intermediate. Biochemistry 1994; 33: 8375–83.

Safar J, Wille H, Itri V, Groth D, Serban H, Torchia M, et al. Eight prion strains have PrP^{Sc} molecules with different conformations. Nat Med 1998; 4: 1157–65.

Safar JG. Molecular Mechanisms Encoding Quantitative and Qualitative Traits of Prion Strains. In: Gambetti P, editor. Prions and diseases. New York: Springer Verlag; 2012a.

Safar JG. Molecular pathogenesis of sporadic prion diseases in man. Prion 2012b; 6: 108–15.

Safar JG, Geschwind MD, Deering C, Didorenko S, Sattavat M, Sanchez H, et al. Diagnosis of human prion disease. Proc Natl Acad Sci USA 2005; 102: 3501–6.

Safar JG, Lessard P, Tamguney G, Freyman Y, Deering C, Letessier F, et al. Transmission and detection of prions in feces. J Infect Dis 2008; 198: 81–9.

Safar JG, Scott M, Monaghan J, Deering C, Didorenko S, Vergara J, et al. Measuring prions causing bovine spongiform encephalopathy or chronic wasting disease by immunoassays and transgenic mice. Nat Biotechnol 2002; 20: 1147–50.

Sanger F, Nicklen S, Coulson AR. DNA sequencing with chain-terminating inhibitors. Proc Natl Acad Sci USA 1977; 74: 5463–7.

Schellenberg GD, Montine TJ. The genetics and neuropathology of Alzheimer's disease. Acta Neuropathol 2012; 124: 305–23.

Schmidt C, Artjomova S, Hoeschel M, Zerr I. CSF prion protein concentration and cognition in patients with Alzheimer disease. Prion 2013; 7: 229–34.

Schmidt C, Haik S, Satoh K, Rabano A, Martinez-Martin P, Roeber S, et al. Rapidly progressive Alzheimer's disease: a multicenter update. J Alzheimers Dis 2012; 30: 751–6.

Schmidt C, Redyk K, Meissner B, Krack L, von Ahsen N, Roeber S, et al. Clinical features of rapidly progressive Alzheimer's disease. Dement Geriatr Cogn Disord 2010; 29: 371–8.

Schmidt C, Wolff M, Weitz M, Bartlau T, Korth C, Zerr I. Rapidly progressive Alzheimer disease. Arch Neurol 2011; 68: 1124–30.

Selkoe DJ. Alzheimer's disease. Cold Spring Harb Perspect Biol 2011; 3:pii: a004457.

Sherman MA, Lesne SE. Detecting abeta*56 oligomers in brain tissues. Methods Mol Biol 2011; 670: 45–56.

Shirley BA, editor. Protein stability and folding: theory and practice. Totowa, New Jersey: Humana Press; 1995.

Steensgaard J, Humphries S, Spragg SP. Measurements of sedimentation coefficients. In: Rickwood D, editor. Preparative centrifugation: a practical approach. Oxford: IRL Press; 1992. p. 187–232.

Stine WB, Jungbauer L, Yu C, LaDu MJ. Preparing synthetic Abeta in different aggregation states. Methods Mol Biol 2011; 670: 13–32.

Tatsuoka C, Tseng H, Jaeger J, Varadi F, Smith MA, Yamada T, et al. Modeling the heterogeneity in risk of progression to Alzheimer's disease across cognitive profiles in mild cognitive impairment. Alzheimers Res Ther 2013; 5: 14.

Thackray AM, Hopkins L, Bujdoso R. Proteinase K-sensitive disease-associated ovine prion protein revealed by conformation-dependent immunoassay. Biochem J 2007; 401: 475–83.

Tycko R. Molecular structure of amyloid fibrils: insights from solid-state NMR. Q Rev Biophys 2006; 39: 1–55.

Wilkosz PA, Seltman HJ, Devlin B, Weamer EA, Lopez OL, DeKosky ST, et al. Trajectories of cognitive decline in Alzheimer's disease. Int Psychogeriatr 2010; 22: 281–90.

Wille H, Prusiner SB. Ultrastructural studies on scrapie prion protein crystals obtained from reverse micellar solutions. Biophys J 1999; 76: 1048–62.

Ye BS, Seo SW, Cho H, Kim SY, Lee JS, Kim EJ, et al. Effects of education on the progression of early- versus late-stage mild cognitive impairment. Int Psychogeriatr 2013; 25: 597–606.